ACS Medicinal Chemistry Letters

pubs.acs.org/acsmedchemlett

Letter

Development of Novel Bacterial Topoisomerase Inhibitors Assisted by Computational Screening

Joshua W. Powell, Chelsea A. Mann, Paul D. Toth, Sheri Nolan, Anja Steinert, Clarissa Ove, Justin T. Seffernick, Daniel J. Wozniak, Razieh Kebriaei, Steffen Lindert, Neil Osheroff, Jack C. Yalowich, and Mark J. Mitton-Fry*

Cite This: *ACS Med. Chem. Lett.* 2024, 15, 1287−1297

Read Online

ACCESS | Metrics & More | Article Recommendations | Supporting Information

ABSTRACT: Multidrug-resistant bacterial infections pose an ever-evolving threat to public health. Since the outset of the antibacterial age, bacteria have developed a multitude of diverse resistance mechanisms that suppress the effectiveness of current therapies. New drug entities, such as Novel Bacterial Topoisomerase Inhibitors (NBTIs), can circumvent this major issue. A computational docking model was employed to predict the binding to DNA gyrase of atypical NBTIs with novel pharmacophores. Synthesis of NBTIs based on computational docking and subsequent antibacterial evaluation against both Gram-positive and Gram-negative bacteria yielded congeners with outstanding anti-staphylococcal activity and varying activity against select Gram-negative pathogens.

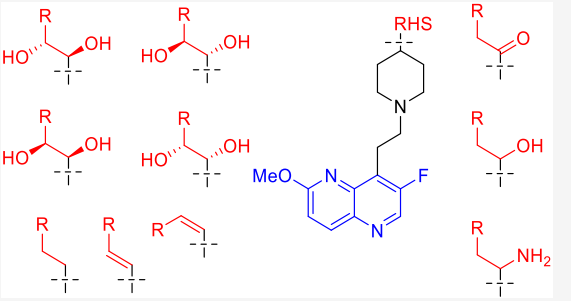

KEYWORDS: *MRSA, gyrase, antimicrobial resistance, cleavage, efflux*

Antibacterial resistance is an ever-growing threat to humanity. The essential bacterial topoisomerase enzymes, DNA gyrase[1] and topoisomerase IV (TopoIV),[2] are attractive targets, as exemplified by the fluoroquinolone class of antibacterials. However, a rapid increase in resistance in recent decades, driven primarily by mutations to the genes encoding the topoisomerase targets, has reduced their effectiveness.[3,4] One strategy to attack such resistant bacteria is to target these essential enzymes at novel binding sites. Novel Bacterial Topoisomerase Inhibitors (NBTIs), such as gepotidacin (now known as a triazaacenaphthylene), elude fluoroquinolone resistance using this strategy and display a differentiated pharmacological profile.[5]

The pharmacophore of gepotidacin is typical for most NBTIs (see Figure 1).[5,6] The left-hand side (LHS, blue) utilizes either a bi- or tricyclic ring system to bind bacterial DNA. The linker (black) connects the LHS and the right-hand side (RHS, red), a moiety binding to a hydrophobic pocket in the topoisomerase. The RHS secondary amine is prototypical and interacts with a highly conserved aspartate (D83, *Staphylococcus aureus* numbering) in the GyrA subunit of DNA gyrase, at the entrance to the binding pocket.[7,8] A mono- or bicyclic ring system binds nonspecifically to this pocket. The binding mode identified by X-ray crystallographic studies has been further validated by selection for NBTI-resistant mutants, of which GyrA D83N is common.[9] Extensive optimization efforts have varied each portion of the pharmacophore, with the aims of improving antibacterial activity, enhancing pharmacokinetic properties, and reducing key safety liabilities including hERG inhibition.[5,6]

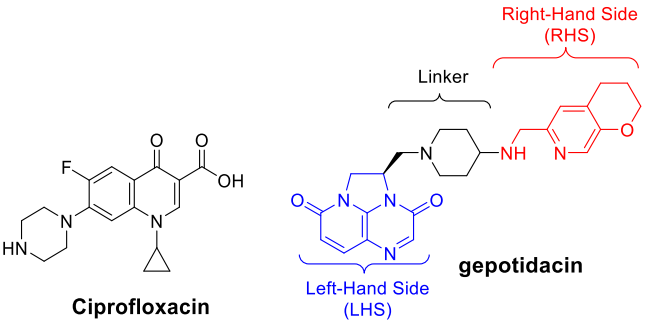

Figure 1. Examples of a fluoroquinolone (ciprofloxacin) and NBTI (gepotidacin) are shown, with the key elements of the NBTI pharmacophore highlighted.

In this study, we have combined experimental results from previously synthesized molecules with a computational model to predict binding affinities of novel structures, enabling evaluation and prioritization of unique RHS pharmacophores prior to synthesis. In doing so, we identified atypical NBTIs with potent Gram-positive antibacterial activity. Gram-negative activity has

Received: April 11, 2024
Revised: June 16, 2024
Accepted: June 20, 2024
Published: July 15, 2024

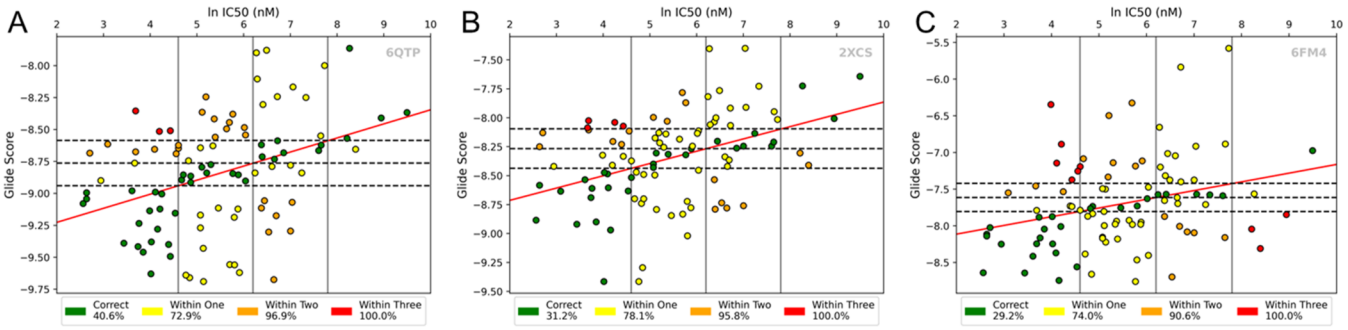

Figure 2. Assessing the predictive accuracy of docking results using binned classification: binning assessment of systems selected from benchmarking: (**A**) 6QTP, (**B**) 2XCS, and (**C**) 6FM4. For a series of known NBTIs, the predicted binding score was plotted versus the natural logarithm of the measured IC_{50} value from a *S. aureus* DNA gyrase supercoiling assay. Agreement between experimental values and average Glide docking score was measured to determine the predictive accuracy of each DNA gyrase system (green: correct; yellow: within one bin; orange: within two; red: within three).

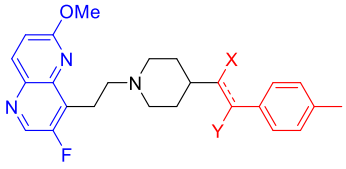

Figure 3. General structure of the targeted compounds.

Table 1. Predicted Binding Scores of Atypical NBTIs

RHS	Avg Z-Score	RHS	Avg Z-Score
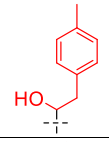	-1.510	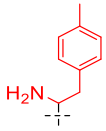	-1.907
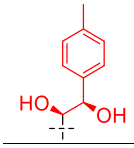	-1.012	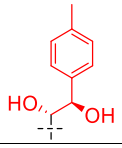	-1.210
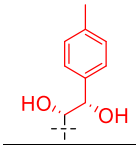	-1.012	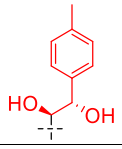	-1.210

proven more challenging, with efflux posing a particular challenge, as has been observed previously.[5,10]

Our efforts began with a set of 96 compounds, for which we had experimentally determined IC_{50} values for inhibition of gyrase-mediated supercoiling, which were used as a rough surrogate for binding affinity. Using Schrödinger Glide,[11] each compound was docked into seven receptors constructed from high-resolution DNA gyrase crystals with bound NBTIs: PDB IDs 2XCS, 4PLB, 5BS3, 5NPP, 6FM4, 6QTK, and 6QTP. An initial self-docking screening was conducted to evaluate the utility of each crystal as a docking receptor (Figure S1, Supporting Information [SI]). For each of these systems, we created four experimental binding affinity bins based on the ln IC_{50} (nM) values of the benchmark compounds with bounds at 4.6 (100 nM), 6.2 (500 nM), and 7.8 (2500 nM). We then calculated least-squares linear regressions from the Glide docking data and natural log IC_{50} values of each receptor. A second set of cutoffs to represent docking scores was then defined, where the regressions intersected the IC_{50} bounds. This gave us a total of 16 bins, into which the benchmark compounds fell (Figure 2). We could subsequently evaluate the performance of each system based on the number of benchmark compounds that had a matching docking score and IC_{50} bins. Those along the positive diagonal had consistent experimental and computational classifications, i.e., both values were ranked excellent or both poor. These compounds were categorized as "correctly predicted." The inhibitors that fell outside of these diagonal bins,

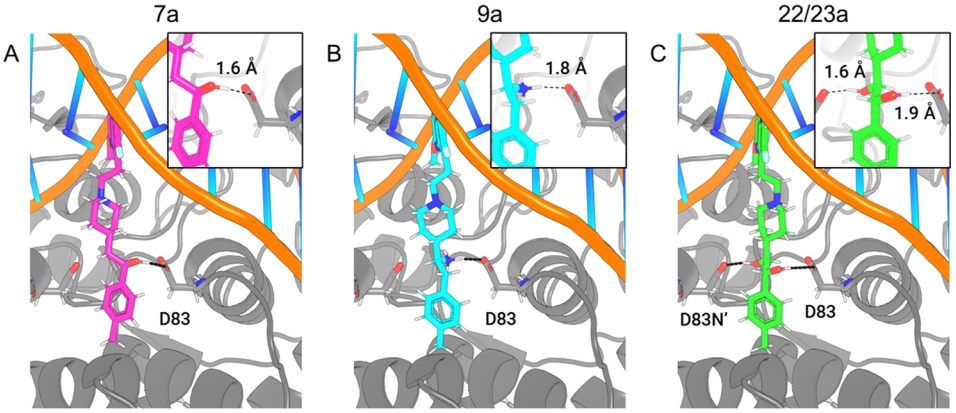

Figure 4. Predicted docking poses and interactions with GyrA D83 in 2XCS of (**A**) monohydroxyl (**7a**) (1.6 Å to D83), (**B**) primary amine (**9a**) (1.8 Å to D83), and (**C**) *anti*-diol (**22**/**23a**) (1.6 and 1.9 Å to D83).

https://doi.org/10.1021/acsmedchemlett.4c00162
ACS Med. Chem. Lett. 2024, 15, 1287−1297

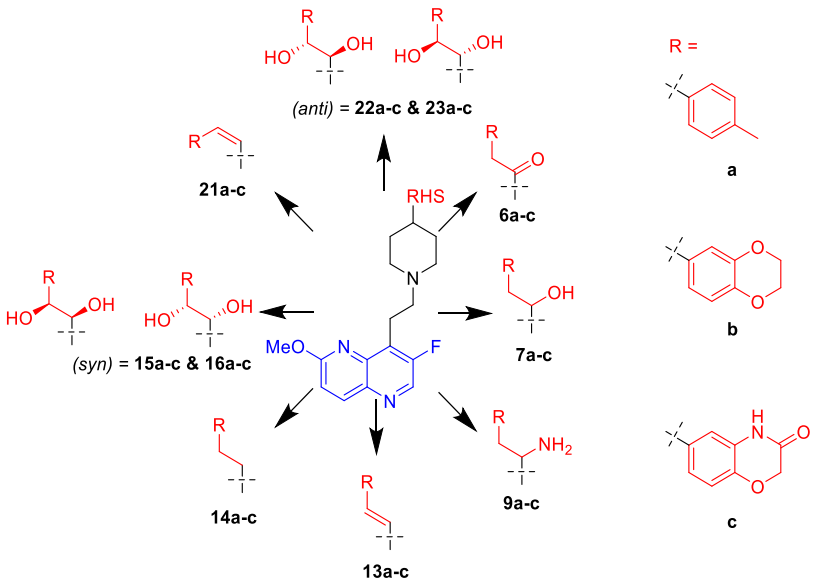

Figure 5. Overview of synthesized compounds.

Scheme 1. Synthesis of Ketones and Monohydroxyls, and Primary Amines[a]

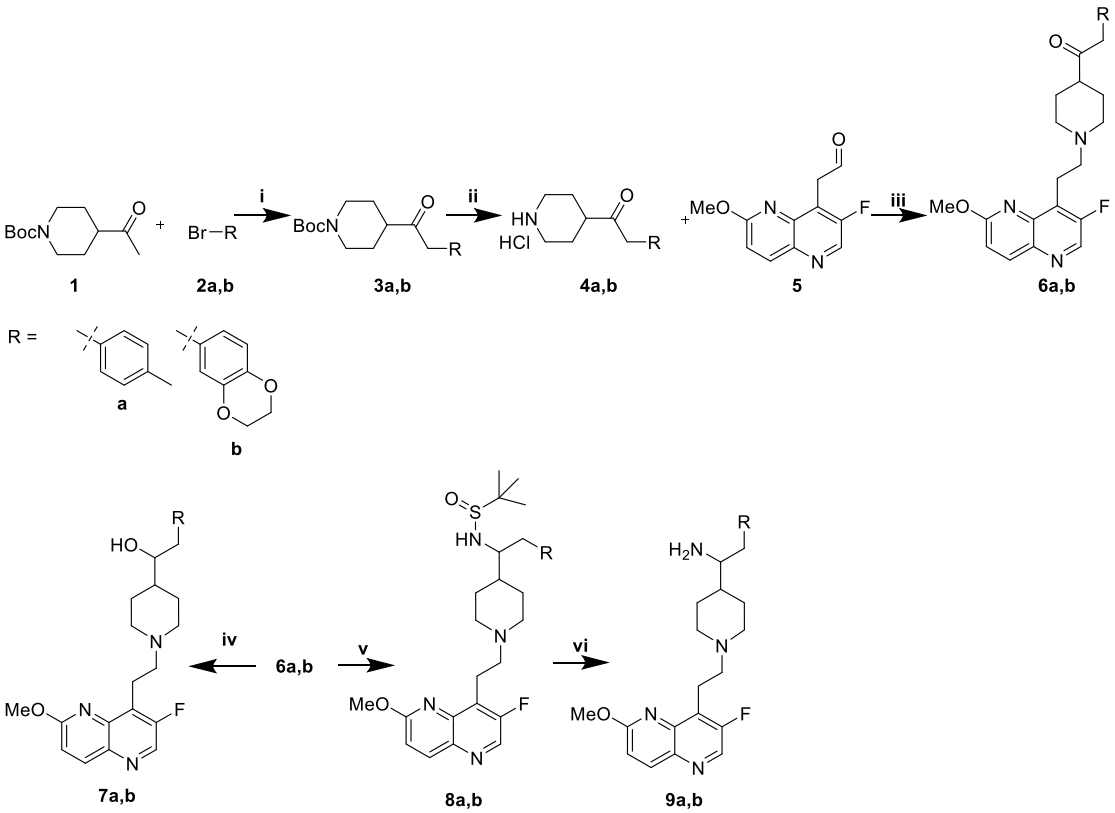

[a]Reaction conditions: (i) NaO^{t}Bu, Pd_2dba_3, (±)-BINAP, THF, 70 °C; (ii) HCl, MeOH; (iii) 1. AcOH, THF/MeOH, 4 Å MS. 2. $NaCNBH_3$; (iv) $NaBH_4$, MeOH; (v) 1. $H_2NSOC(CH_3)_3$, $Ti(OEt)_4$, THF, 70 °C. 2. $NaBH_4$, MeOH; (vi) HCl, MeOH.

where the experimental and computational classifications did not agree, were "incorrectly predicted". Depending on the number of bins by which the docking classification deviated from the ln IC_{50} classification, they were labeled as "within one", "within two", or "within three" of their correct bin.

Three systems were identified for downstream analysis based on a combination of their ability to predict compounds as "within one" or better and the R^2 of their regression line: 6QTP (R^2: 0.14, correct: 40.6%, within one bin: 72.9%), 2XCS (R^2: 0.16, correct: 31.2%, within one bin: 78.1%), and 6FM4 (R^2: 0.08, correct: 30%, within one bin: 74.0%). These were then used to screen all potential synthesis candidates as an initial evaluation. Docking score distributions of the 443 compounds tested are shown in Figure S2, SI. As docking scores cannot be directly compared across different structures, the results from all systems were normalized to Z-scores (see Equation S1, SI) as

https://doi.org/10.1021/acsmedchemlett.4c00162
ACS Med. Chem. Lett. 2024, 15, 1287−1297

Scheme 2. Synthesis of (*E*)-Olefins, Alkanes, and *Syn*-Diols[a]

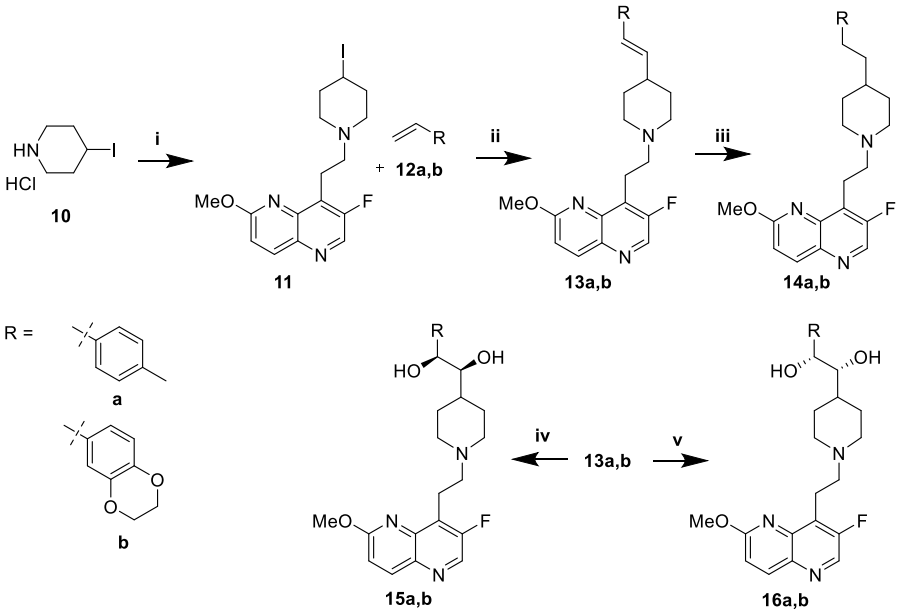

[a]Reaction conditions: (i) 1. **5**, AcOH, THF/MeOH, 4 Å MS. 2. $NaCNBH_3$; (ii) 4-CZIPN, $Co(dmgH)(dmgH_2)Cl_2$, HK_2PO_4, Et_3N, DMF, 440 nm light; (iii) H_2, 10% Pd/C, EtOH; (iv) AD-mix-α, ^{t}BuOH/water; (v) AD-mix-β, ^{t}BuOH/water.

Scheme 3. Synthesis of (*Z*)-Olefins and *Anti*-Diols[a]

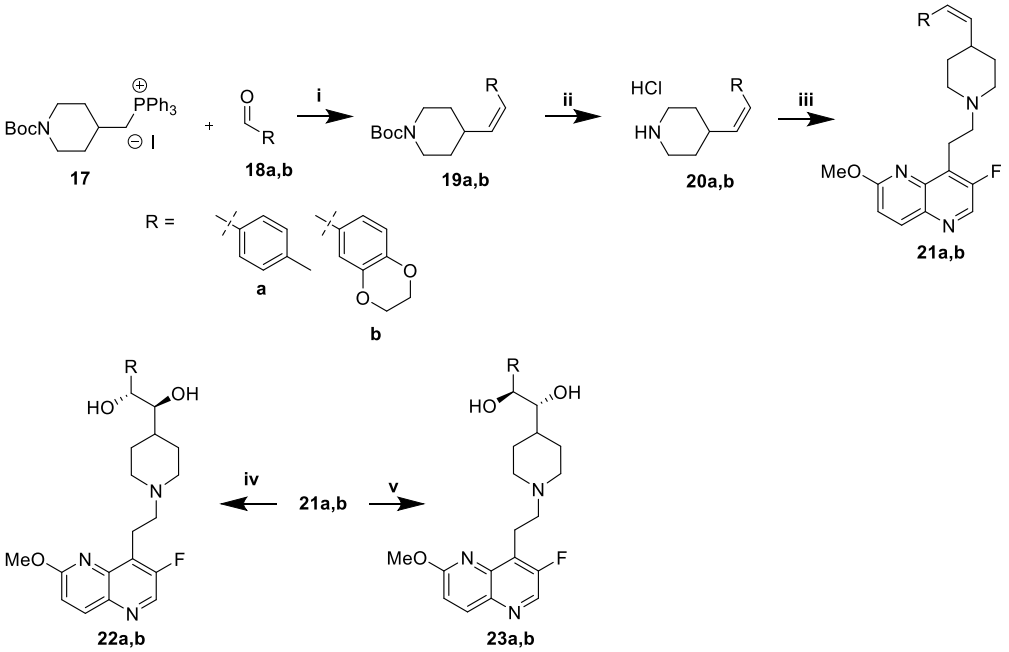

[a]Reaction conditions: (i) KO^{t}Bu, THF, 0 °C; (ii) HCl, MeOH; (iii) 1. **5**, AcOH, THF/MeOH, 4 Å MS. 2. $NaCNBH_3$; (iv) AD-mix-α, ^{t}BuOH/water; (v) AD-mix-β, ^{t}BuOH/water.

seen in previous publications.[12−14] Compounds were selected for synthesis and experimental analysis based on the average of their Z-scores across the three systems mentioned above, with more negative values reflecting better predicted binding.

To simplify the workflow, docking experiments were conducted with targeted variations in the RHS moiety while holding other components consistent (Figure 3 and Table 1). Docking of the "traditional" NBTI with a secondary amine (**40**) afforded an average Z-score of −0.949, and novel structures with superior (more negative) scores were prioritized for synthesis and experimental evaluation. In this research, our molecular design strategy focused on replacement of the secondary amine with other functional groups capable of engaging GyrA D83; four classes of analogues were of particular interest (alcohol **7a−c**, *syn*- and *anti*-diols (**15a−c** and **16a−c**; **22a−c** and **23a−c**), and primary amine (**9a−c**) (Figure 5). Primary amines have been associated with increased intracellular accumulation and reduced efflux in Gram-negative bacteria,[10,15] and our chosen compound set enables a matched-pair comparison of primary amines with analogous alcohols and the secondary amine.

https://doi.org/10.1021/acsmedchemlett.4c00162
ACS Med. Chem. Lett. 2024, 15, 1287−1297

Scheme 4. Synthesis of Alkane and Alkenes with Oxazinone RHS[a]

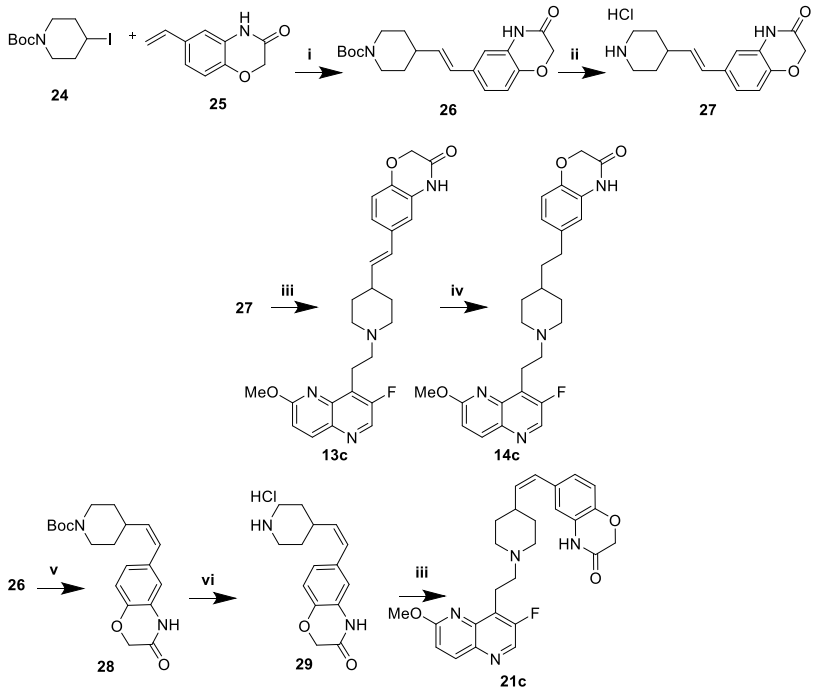

[a]Reaction conditions: (i) 4-CZIPN, $Co(dmgH)(dmgH_2)Cl_2$, HK_2PO_4, Et_3N, DMF, 440 nm light; (ii) HCl, MeOH; (iii) 1. **5**, AcOH, THF/MeOH, 4 Å MS. 2. $NaCNBH_3$; (iv) H_2, 10% Pd/C, MeOH; (v) $(Ir[dF(CF_3)ppy]_2(dtbpy))PF_6$, ACN, 456 nm light; (vi) HCl, MeOH.

Scheme 5. Synthesis of *Syn*- and *Anti*-Diols with Oxazinone RHS[a]

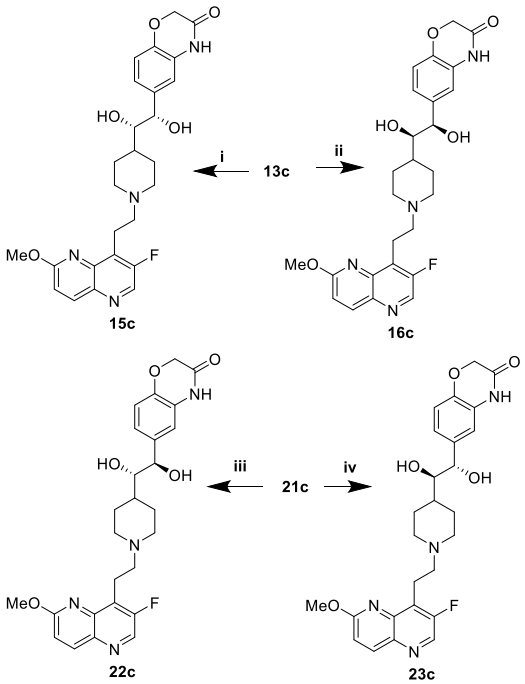

[a]Reaction conditions: (i) AD-mix-α, ^{t}BuOH/water; (ii) AD-mix-β, ^{t}BuOH/water; (iii) AD-mix-α, ^{t}BuOH/water; (iv) AD-mix-β, ^{t}BuOH/water.

Predicted docking poses (Figure 4) display interactions with the D83 residue at the entrance to the binding pocket of DNA gyrase. This prediction is in line with the known binding mode of traditional NBTIs.[5−8] The diol (**22**/**23a**) and monohydroxyl (**7a**) form a hydrogen bonding interaction, while the amine (**9a**) forms an ionic interaction. Within each compound class, analogues with three diverse RHS moieties were synthesized, the hydrophobic *para*-toluyl group (**a**), the more polar benzodioxane possessing two potential hydrogen bond acceptors (**b**), and benzoxazinone (**c**) containing both hydrogen bond donor and acceptor moieties. The compounds shared similar synthetic routes. Moreover, antibacterial testing of various intermediates, namely, ketones (**6a−c**), (*E*)-olefins (**13a−c**), and (*Z*)-olefins (**21a−c**) as well as the readily accessible alkanes (**14a−c**) further expanded our understanding of structure−activity relationships.

The tolyl and benzodioxane compounds were prepared by analogous routes (Schemes 1−3), while the oxazinones generally necessitated modified approaches (Schemes 4−7).

Ketone (**6a**,**b**), monohydroxyl (**7a**,**b**), and primary amine (**9a**,**b**) analogues were prepared from ketone **1** (Scheme 1). Preliminary studies (not shown) indicated little dependence of the antibacterial activity on the absolute stereochemistry of the monohydroxyl or primary amine compounds. Consequently, racemic mixtures were synthesized. Pd-catalyzed arylation with the requisite aryl bromides **2a**,**b** afforded intermediates **3a**,**b**. Boc deprotection with methanolic HCl yielded amines **4a**,**b** as hydrochloride salts. Reductive amination of aldehyde **5** afforded ketones **6a**,**b**. Reduction with $NaBH_4$ provided racemic monohydroxyls **7a**,**b**, whereas reductive amination with racemic *tert*-butylsulfinamide provided sulfinamide intermediates **8a**,**b**. Acidic deprotection afforded racemic primary amines **9a**,**b**.

The synthesis of (*E*)-alkene **13a**,**b**, alkane **14a**,**b**, and *syn*-diol compounds (**15a**,**b** and **16a**,**b**) began with reductive amination of aldehyde **5** with 4-iodopiperidine **10** to afford intermediate **11** (Scheme 2). A Heck-type coupling under photocatalytic conditions with styrenes **12a**,**b** produced the (*E*)-olefins **13a**,**b** stereoselectively (dr >10:1).[16] Hydrogenation afforded alkanes

https://doi.org/10.1021/acsmedchemlett.4c00162
ACS Med. Chem. Lett. 2024, 15, 1287−1297

Scheme 6. Synthesis of Ketone, Monohydroxyl, and Monoamine with Oxazinone RHS[a]

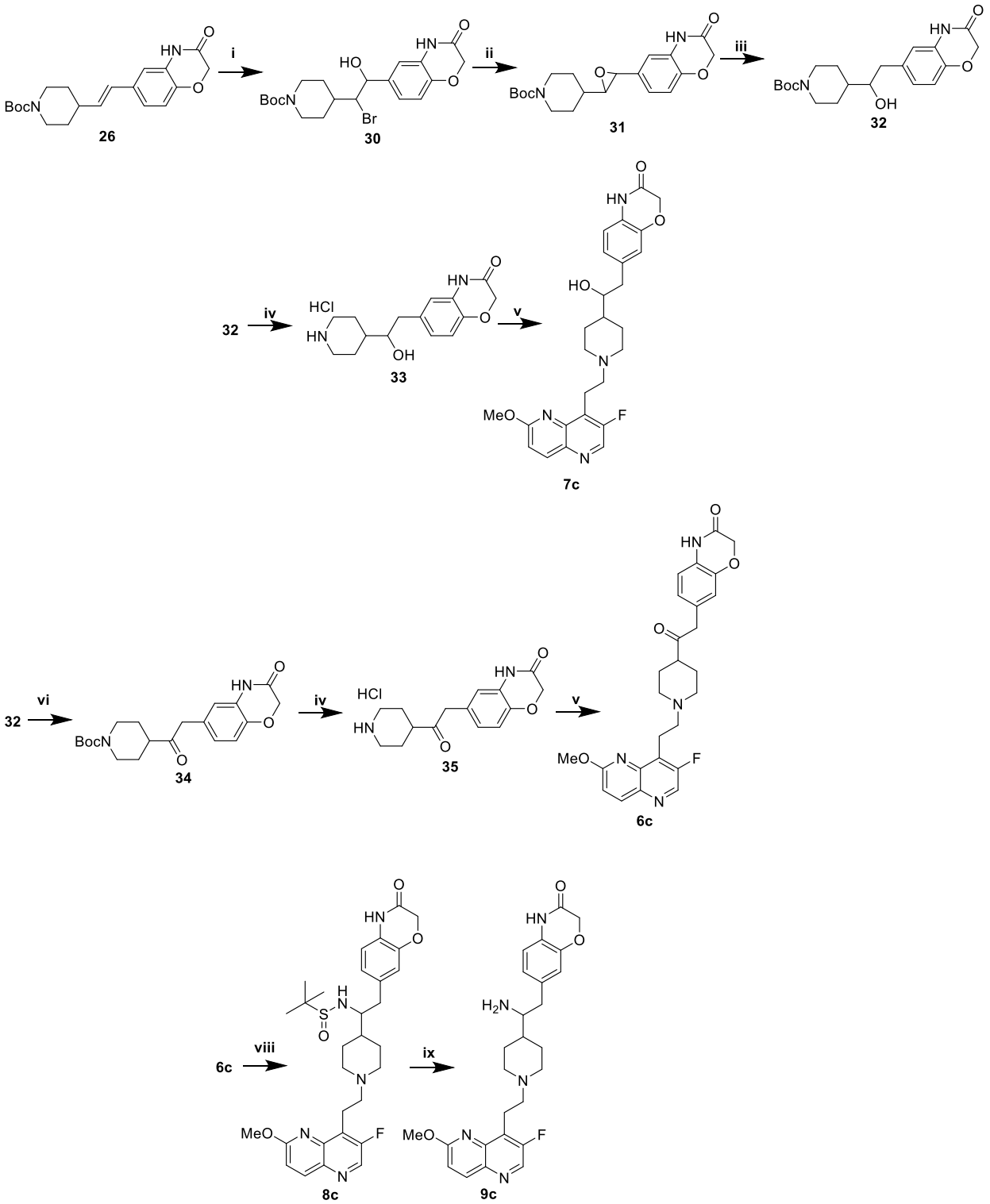

[a]Reaction conditions: (i) NBS, ACN/water; (ii) K_2CO_3, MeOH; (iii) H_2, 10% Pd/C, EtOH; (iv) HCl, MeOH; (v) 1. **5**, AcOH, THF/MeOH, 4 Å MS. 2. $NaCNBH_3$; (vi) DMP, DCM; (vii) HCl, MeOH; (viii) 1. $H_2NSOC(CH_3)_3$, $Ti(OEt)_4$, THF, 2. $NaBH_4$, MeOH; (ix) HCl, MeOH..

14a,b. Alternatively, Sharpless asymmetric dihydroxylation of the (*E*)-olefins using commercially available AD-mix-α or -β provided *syn*-diols **15a,b** and **16a,b**, respectively.

The synthesis of (*Z*)-alkene **21a,b** and *anti*-diol compounds (**22a,b** and **23a,b**) began with Wittig reaction of **17** with commercially available aldehydes **18a,b** to afford (*Z*)-alkene intermediates **19a,b** in high stereoselectivity (dr ∼25:1, Scheme 3). Boc deprotection to afford **20a,b** and subsequent reductive amination of aldehyde **5** yielded (*Z*)-alkenes **21a,b**. Sharpless asymmetric dihydroxylation using AD-mix-α or -β delivered *anti*-diols **22a,b** and **23a,b**, respectively.

https://doi.org/10.1021/acsmedchemlett.4c00162
ACS Med. Chem. Lett. 2024, 15, 1287−1297

Scheme 7. Synthesis of Secondary Amine[a]

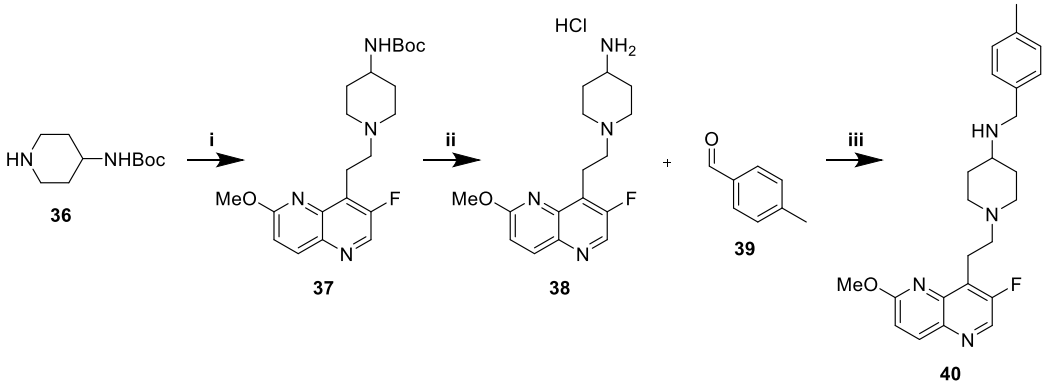

[a]Reaction conditions: (i) 1. **5**, AcOH, THF/MeOH, 4 Å MS. 2. $NaCNBH_3$; (ii) HCl, MeOH; (iii) AcOH, THF/MeOH, 4 Å MS. 2. $NaCNBH_3$.

The synthesis of benzoxazinone-type analogues was generally more difficult owing to the presence of an abstractable proton, requiring modified routes. Heck-type coupling of iodide **24** and styrene **25** under photocatalytic conditions afforded (*E*)-alkene **26** (Scheme 4).[16] Boc deprotection to afford **27**, followed by reductive amination with **5**, yielded (*E*)-olefin **13c**, which was hydrogenated to provide **14c**. Alternatively, photocatalytic isomerization of (*E*)-olefin **26** at 456 nm with iridium catalysis afforded (*Z*)-olefin **28**. Boc deprotection to provide **29** and subsequent reductive amination of aldehyde **5** yielded (*Z*)-olefin **21c**.

The *syn*- (**15c**, **16c**) and *anti*-diols (**22c**, **23c**) were prepared via Sharpless asymmetric dihydroxylation of the (*E*)- and (*Z*)-alkenes, respectively (Scheme 5).

Ketone **6c**, monohydroxyl **7c**, and primary amine **9c** were synthesized beginning with (*E*)-alkene **26** (Scheme 6). Reaction with NBS afforded bromohydrin **30**, which was converted to epoxide **31** under basic conditions. Hydrogenolysis using 10% Pd/C provided alcohol **32**. Deprotection with methanolic HCl afforded piperidine **33**, and reductive amination of aldehyde **5** yielded monohydroxylated analogue **7c**. Alternatively, the oxidation of **32** with Dess-Martin periodinane yielded ketone **34**. Acidic Boc deprotection to provide piperidine **35** and reductive amination with aldehyde **5** afforded ketone analogue **6c**. Reductive amination of the ketone with racemic *tert*-butylsulfinamide afforded **8c**, and a final deprotection with methanolic HCl provided racemic primary amine **9c**.

A single secondary amine **40** was synthesized as a comparator representing the "traditional" NBTI scaffold (Scheme 7). Aldehyde **5** and piperidine **36** were reacted via reductive amination to afford Boc protected **37**. Deprotection under acidic conditions and reductive amination with aldehyde **39** produced secondary amine **40**.

Minimal inhibitory concentrations (MICs) were determined using three strains of *S. aureus* and two Gram-negative pathogens (*Escherichia coli* and *Acinetobacter baumannii*). The strains of *S. aureus* include one wildtype (ATCC 29213), one NBTI-resistant (GyrA D83N amino acid substitution[17]), and one fluoroquinolone-resistant MRSA (USA300).

Surprisingly, (*E*)-olefins **13a−c** and alkanes **14a−c** displayed anti-staphylococcal activity, suggesting that NBTIs do not absolutely require the prototypical interaction with D83 at the entrance of the DNA gyrase binding pocket if the appropriate binding vector is achieved. Meanwhile, (*Z*)-olefins **21a−c** did not retain the same activity, perhaps due to the misorientation of the RHS by the bond angle produced by the (*Z*)-olefin. Monohydroxylated compounds **7a−c** were more potent than the alkanes and alkenes and were comparable to other synthesized compounds when comparing Gram-positive MICs. This finding was also intriguing, as the monohydroxyls are incapable of forming an ionic interaction with D83 but can hydrogen bond, as predicted in Figure 4. Ketones (**6a** and **6c**) were similarly active vs *S. aureus*, whereas compound **6b** showed elevated MICs. Primary amines **9a−c** were less potent than matched monohydroxyls **7a−c**. The computational model (Table 1) predicted equivalent GyrA binding between diol enantiomers. Table 2 results confirmed this prediction: only minimal differences were observed for S. *aureus* [ATCC 29213, USA300 (MRSA)] MICs in head-to-head comparisons of **15a**,**b** with **16a**,**b** or **22a−c** with **23a−c**. Results for **15c** and **16c** were within the standard variability in the MIC assays. In contrast, docking results (Table 1) predicted a greater GyrA binding affinity for the *anti*- (**22a−c** and **23a−c**) versus the *syn*-diols (**15a−c** and **16a−c**). Results in Table 2 were consistent with this prediction, with *S. aureus* [ATCC 29213, USA300 (MRSA)] MICs values indicating improved activity for the *anti*- compared to the *syn*-diol analogues.

All compounds lost activity in the NBTI-resistant strain (GyrA D83N) suggesting that the atypical NBTIs described here derive their antibacterial activity primarily from targeting DNA gyrase. The loss of activity for (*E*)-alkenes, alkanes, and (*Z*)-alkenes is particularly striking, given that they are incapable of direct interaction with D83. The precise origins of this effect are not fully understood. The analogous GyrA D82N mutation is in *E. coli* leads to diminished target inhibition by fluoroquinolones and imidazopyrazinones,[19] neither of which directly contacts the aspartate. This observation has been attributed to reductions in the ability of gyrase to cleave DNA.

Compared to *S. aureus*, the MICs for these atypical NBTIs against Gram-negative pathogens were elevated. However, several structure−activity relationships were observed. Oxazinone-containing compounds often outperformed other RHS moieties (e.g., **6c**, **7c**, **13c**, and **14c**). Incorporating primary amines has previously been associated with a higher intracellular accumulation in *E. coli*.[10,15] In contrast with their diminished anti-staphylococcal activity, primary amines (**9a−c**) displayed comparable *E. coli* MICs to the matched monohydroxyls (**7a−c**), potentially reflecting improved accumulation. Primary amine **9a** was 4-fold less potent than the structure-matched secondary amine control (**40**) for both Gram-negative bacteria. As with *S. aureus*, MICs for (*Z*)-olefins (**21a−c**) were higher, whereas those of (*E*)-olefins (**13b**,**c**) were similar to other chemotypes.

https://doi.org/10.1021/acsmedchemlett.4c00162
ACS Med. Chem. Lett. 2024, 15, 1287−1297

Table 2. Minimal Inhibitory Concentrations (μg/mL) of Atypical NBTIs[a]

Cmpd	*S. aureus* ATCC 29213	*S. aureus* D83N[b]	*S. aureus* USA300 (MRSA)	*E. coli* ATCC 25922	*A. baumannii* ATCC 19606
Ketones					
6a	0.13	4	0.13	16	32
6b	4	32	4	64	64
6c	≤0.13	16	≤0.13	2	4
Monohydroxyls					
7a	0.06	8	0.25	16	32
7b	0.25	4	0.25	8	8
7c	≤0.13	16	≤0.13	4	4
Primary amines					
9a	1	32	4	16	16
9b	2	≥16	4	8	16
9c	16	64	8	8	32
(*E*)-**Alkenes**					
13a	0.25−0.5[c]	≥32	0.5	≥64	≥64
13b	0.25	2	0.5	8	8
13c	0.5	16	≤0.25	4	8
Alkanes					
14a	0.5	4	0.5	64	64
14b	0.5	8	1	16	32
14c	1	32	0.5	4	8
(*syn*)-**Diols**					
15a	1−2[c]	≥32	2−4[c]	64	32−64[c]
15b	1	≥32	2	32	16
15c	1	≥32	1	32	16
16a	1	≥32	2	64	64
16b	1−4[c]	16	1−4[c]	16	8−16[c]
16c	8	≥32	8	16	32
(*Z*)-**Alkenes**					
21a	4−8[c]	32	4−8[c]	≥64	≥64
21b	8	≥16	8	≥64	64
21c	≥64	≥64	64	64	32
(*anti*)-**Diols**					
22a	0.13	16	0.13	16	16
22b	≤0.13	16	0.25	16	8
22c	2	64	4	8	32
23a	0.13	≥32	0.25	32	16
23b	0.03	8	0.03	8	4
23c	2	64	2	8	32
Controls					
40	≤0.25	16	≤0.25	4	4
Gep.[d]	0.125−1[c]	8−32[c]	0.125−0.5[c]	1−4[c]	8−32[c]
Cipro.[d]	0.25−0.5[c]	0.25−1[c]	16−64[c]	0.0075−0.25[c]	1−2[c]

[a]Minimal inhibitory concentrations (MICs) determined in triplicate (at a minimum) according to CLSI guidelines.[18] [b]First-step mutant of *S. aureus* 29213.[17] [c]Ranges of observed values given where appropriate. [d]Gepotidacin and ciprofloxacin employed as controls.

The *syn*- (**15a−c** and **16a−c**) and *anti*-diols (**22a−c** and **23a−c**) had comparable activity against Gram-negative pathogens. Overall, the compounds displayed more modest antibacterial activity against the studied Gram-negative pathogens, as is commonly seen with NBTIs,[5,17] albeit with some exceptions.[20] We suspect that the reduced activity may be due to lower intracellular accumulation as a result of efflux (see below).

To address the question of efflux, compounds were tested against wildtype and efflux-deficient strains of *Salmonella enterica* serovar Typhimurium (Table 3), a clinically important Gram-negative pathogen causing salmonellosis.[21] The tolC-knockout lacks a prominent efflux channel present in the wildtype.[22] By comparing the MICs for both strains, we can estimate the impact of the efflux.

Whereas compounds displayed poor activity against the wildtype strain, MICs were significantly improved against the efflux-deficient strain. Primary amines **9a−c** displayed reduced susceptibility to efflux, with 8- to 16-fold changes observed between strains, whereas changes for other compounds ranged as high as 512-fold. Thus, the primary amines are not effluxed as efficiently as other chemotypes,[15] as has been previously observed in a structurally distinct series of NBTIs.[10]

Biochemical evaluations using isolated bacterial topoisomerases were conducted to validate the mechanism of action and further support the MIC results and the computational model. The inhibition of supercoiling by *S. aureus* DNA gyrase was measured as previously described.[25] The secondary amine control (**40**), monohydroxyl (**7a**), monoamine (**9a**), and *anti*-diol (**22a**) were chosen as representative compounds, holding

https://doi.org/10.1021/acsmedchemlett.4c00162
ACS Med. Chem. Lett. 2024, 15, 1287−1297

Table 3. Antibacterial Activity vs *Salmonella* Strains[a]

Cmpd	*S. enterica* Typhimurium ATCC 14028 MIC (μg/mL)	*S. enterica* Typhimurium 14028 Δ*tolC1*::kan[b] MIC (μg/mL)	Fold Change
6a	64	0.5	128
6b	≥64	1 to >1[c]	≥64
6c	16	≤0.125	≥128
7a	64	1	64
7b	32	0.25	128
7c	16	≤0.125	≥128
9a	64	4	16
9b	32	2	16
9c	32	4	8
13a	≥64	0.5−1[c]	≥64
13b	64	0.125	512
13c	16	0.25	64
14a	≥64	1	≥64
14b	64	0.25	256
14c	16	0.5	32
15a	≥64	1−2[b]	≥64
15b	64	1	64
15c	32	0.25	128
16a	≥64	0.5−1[c]	≥128
16b	64	0.5	128
16c	64	1	64
21a	≥64	8	≥8
21b	≥64	4	≥16
21c	64	16	4
22a	64	1	64
22b	32	0.25	128
22c	≥64	8	≥8
23a	64	1	64
23b	32	0.125	256
23c	32	0.5	64
40	32	0.5	64
Gep.[d]	2−8[c]	0.125−0.5[c]	4−16
Cipro.[d]	≤0.13	≤0.13	N/A

[a]Minimal inhibitory concentrations (MICs) determined in triplicate (at a minimum) according to CLSI guidelines.[18] [b]Efflux-deficient strain EFB044. This strain was constructed by moving mutation Δ*tolC1*::kan from the McClelland mutant collection[23] into wildtype strain 14028 using P22 transduction.[24] [c]Ranges of observed values given where appropriate. [d]Gepotidacin and ciprofloxacin employed as controls.

Table 4. Supercoiling IC_{50} against DNA Gyrase and Decatenation IC_{50} Against TopoIV[a]

Cmpd	*S. aureus* DNA gyrase IC_{50} (μM)[a]	*S. aureus* TopoIV IC_{50} (μM)[b]	*S. aureus* TopoIV/ gyrase ratio	E. *coli* DNA gyrase IC_{50} (μM)[a]
7a	0.24	2.29	9.5	12.37
9a	5.05	82.6	16.4	>400
22a	0.065	3.31	50.9	17.09
40	0.004	0.69	176.9	NT[c]

[a]Inhibition of supercoiling activity (n = 3). [b]Inhibition of decatenation activity (n = 3). [c]Not tested.

the LHS and RHS constant to assess the impact of the novel functionality. Secondary amine **40** afforded the most potent inhibition despite its predicted weaker binding (Table 4). For the novel compounds, the relative binding affinities predicted by the computational model (Table 1) were not always consistent with the inhibition of *S. aureus* DNA gyrase, with **9a** being the least potent inhibitor, despite having the best predicted binding affinity. However, the relative whole cell anti-staphylococcal activity followed the same trend as gyrase inhibition (Table 2), supporting DNA gyrase as the principal target in *S. aureus*. Compounds were also evaluated by using *E. coli* DNA gyrase, where inhibition was considerably weaker. The correlation between binding affinities and biochemical inhibition was also less robust, perhaps attributable to the derivation of the docking model from *S. aureus* gyrase structures.

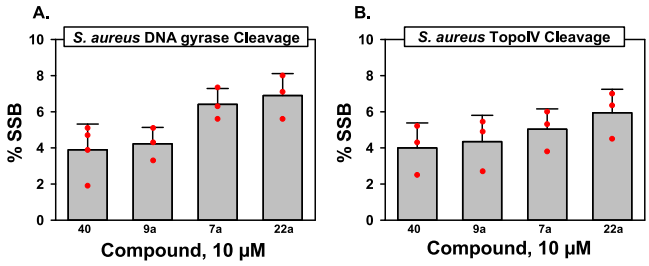

Figure 6. DNA cleavage assays with *S. aureus* DNA gyrase (left, **A**) and TopoIV (right, **B**).

Decatenation experiments with *S. aureus* TopoIV were conducted with the same select compounds to assess the potential for dual targeting of both bacterial topoisomerases. All compounds displayed elevated IC_{50} values for TopoIV over DNA gyrase, and compound **9a** displayed the highest IC_{50} value (Table 4). Compounds **7a** and **22a** had comparable activity in the TopoIV assay, in contrast to their ∼4-fold differences in gyrase IC_{50} values, and **7a** afforded the best TopoIV/gyrase ratio at 9.5. Despite the much higher TopoIV/gyrase ratio for **22a** (51), its potent targeting of DNA gyrase nevertheless afforded excellent anti-staphylococcal activity (Table 2).

NBTIs typically lead to the accumulation of single-strand breaks (SSBs) with both DNA gyrase and TopoIV.[5,7] Given the atypical structures of the NBTIs described herein, an assessment of cleavage activity was warranted. All compounds tested displayed typical NBTI behavior and resulted in an accumulation of SSBs, with minimal to no DSBs observed (<1%, data not shown). For *S. aureus* gyrase at 10 μM, lower levels of SSBs were observed for primary amine **9a** and secondary amine **40** as compared to those of monohydroxyl **7a** and *anti*-diol **22a** (Figure 6A). Similar results were obtained for the TopoIV cleavage assay (Figure 6B).

In this study, we employed a computational docking model to prioritize compounds for the synthesis and testing. Diverse novel chemotypes delivered potent MICs with the Gram-positive pathogen *S. aureus*. Elevated MICs in the NBTI-resistant GyrA D83N mutant *S. aureus* and biochemical testing with isolated enzymes were consistent with gyrase as the primary antibacterial target. Using a test set of three novel chemotypes, we found predicted docking scores were consistent with relative inhibition of *S. aureus* DNA gyrase and with whole cell anti-staphylococcal activity. Antibacterial activity was significantly reduced in Gram-negative bacteria, including *E. coli*, *A. baumannii*, and *S. enterica* Typhimurium. Results from wildtype and efflux-deficient *Salmonella* strains demonstrated that efflux significantly compromised activity in the wildtype strain, indicating a need for continued optimization. In total, these results open the door for further chemical innovation of the NBTI class of antibacterials.

https://doi.org/10.1021/acsmedchemlett.4c00162
ACS Med. Chem. Lett. 2024, 15, 1287−1297

■ ASSOCIATED CONTENT

Supporting Information

The Supporting Information is available free of charge at https://pubs.acs.org/doi/10.1021/acsmedchemlett.4c00162.

Assay methods, computational methods, synthesis and characterization of tested compounds. ^{1}H NMR spectra of tested compounds, ^{13}C NMR spectra, UPLC, and HRMS of selected compounds (PDF)

■ AUTHOR INFORMATION

Corresponding Author

Mark J. Mitton-Fry − *Division of Medicinal Chemistry and Pharmacognosy, The Ohio State University, Columbus, Ohio 43210, United States;* orcid.org/0000-0002-6715-8836; Email: mitton-fry.1@osu.edu

Authors

Joshua W. Powell − *Division of Medicinal Chemistry and Pharmacognosy, The Ohio State University, Columbus, Ohio 43210, United States*

Chelsea A. Mann − *Division of Medicinal Chemistry and Pharmacognosy, The Ohio State University, Columbus, Ohio 43210, United States*

Paul D. Toth − *Department of Chemistry and Biochemistry, The Ohio State University, Columbus, Ohio 43210, United States*

Sheri Nolan − *Microbial Infection and Immunity, The Ohio State University, Columbus, Ohio 43210, United States*

Anja Steinert − *Division of Outcomes and Translational Sciences, The Ohio State University, Columbus, Ohio 43210, United States*

Clarissa Ove − *Division of Medicinal Chemistry and Pharmacognosy, The Ohio State University, Columbus, Ohio 43210, United States*

Justin T. Seffernick − *Department of Chemistry and Biochemistry, The Ohio State University, Columbus, Ohio 43210, United States*

Daniel J. Wozniak − *Microbial Infection and Immunity and Department of Microbiology, The Ohio State University, Columbus, Ohio 43210, United States*

Razieh Kebriaei − *Division of Outcomes and Translational Sciences, The Ohio State University, Columbus, Ohio 43210, United States*

Steffen Lindert − *Department of Chemistry and Biochemistry, The Ohio State University, Columbus, Ohio 43210, United States;* orcid.org/0000-0002-3976-3473

Neil Osheroff − *Department of Biochemistry and Department of Medicine, Vanderbilt University School of Medicine, Nashville, Tennessee 37232, United States;* orcid.org/0000-0002-2550-4884

Jack C. Yalowich − *Division of Pharmaceutics and Pharmacology, The Ohio State University, Columbus, Ohio 43210, United States*

Complete contact information is available at: https://pubs.acs.org/10.1021/acsmedchemlett.4c00162

Funding

Funding was provided by the Dr. Ralph and Marian Falk Medical Research Trust (Transformational Award to M.M-F.) and the NIH (R21 AI148986 and R01 AI173072 to M.M-F. and R01 GM126363 and R01 AI170546 to N.O.).

Notes

The authors declare the following competing financial interest(s): MMF is a shareholder of Pfizer.

■ ACKNOWLEDGMENTS

The authors thank Prof. Daniele Leonori of Aachen University and Dr. Fabio Juliá of Universidad Murcia for their correspondence on the photo-Heck coupling reaction, Drs. Erin Boulanger and Brian Ahmer of The Ohio State University for the *tolC* mutant strain of *Salmonella*, Dr. Yanran Lu for contributing to the biochemical assays, and Jose Orench-Benvenutti for support of MIC assays.

■ ABBREVIATIONS

NBTI, novel bacterial topoisomerase inhibitor; TopoIV, topoiosomerase IV; CLSI, Clinical and Laboratory Standards Institute; SSB, single-strand break; DSB, double-strand break

■ REFERENCES

(1) Gellert, M.; Mizuuchi, K.; O'Dea, M. H.; Nash, H. A. DNA gyrase: An enzyme that introduces superhelical turns into DNA. *Proc. Natl. Acad. Sci. U.S.A.* **1976**, *73* (11), 3872−3876.

(2) Kato, J.; Nishimura, Y.; Imamura, R.; Niki, H.; Hiraga, S.; Suzuki, H. New topoisomerase essential for chromosome segregation in *E. coli*. *Cell.* **1990**, *63* (2), 393−404.

(3) Munita, J. M.; Arias, C. A. Mechanisms of antibiotic resistance. *Microbiol. Spectrum.* **2016**, *4* (2), VMBF-0016-2015.

(4) Aldred, K. J.; Kerns, R. J.; Osheroff, N. Mechanism of Quinolone Action and Resistance. *Biochemistry* **2014**, *53*, 1565−1574.

(5) Kolarič, A.; Anderluh, M.; Minovski, N. Two decades of successful SAR-grounded stories of the novel bacterial topoisomerase inhibitors (NBTIs). *J. Med. Chem.* **2020**, *63* (11), 5664−5674.

(6) Kokot, M.; Anderluh, M.; Hrast, M.; Minovski, N. The Structural Features of Novel Bacterial Topoisomerase Inhibitors that Define Their Activity on Topoisomerase IV. *J. Med. Chem.* **2022**, *65* (9), 6431−6440.

(7) Gibson, E. G.; Bax, B.; Chan, P. F.; Osheroff, N. Mechanistic and structural basis for the actions of the antibacterial gepotidacin against *Staphylococcus aureus* gyrase. *ACS Infect. Dis.* **2019**, *5* (4), 570−581.

(8) Vanden Broeck, A.; Lotz, C.; Ortiz, J.; Lamour, V. Cryo-EM structure of the complete E. coli DNA gyrase nucleoprotein complex. *Nat. Commun.* **2019**, *10*, 4935.

(9) Black, M. T.; Stachyra, T.; Platel, D.; Girard, A. M.; Claudon, M.; Bruneau, J. M.; Miossec, C. Mechanism of action of the antibiotic NXL101, a novel nonfluoroquinolone inhibitor of bacterial type II topoisomerases. *Antimicrob. Agents Chemother.* **2008**, *52* (9), 3339−3349.

(10) Surivet, J.-P.; Zumbrunn, C.; Bruyère, T.; Bur, D.; Kohl, C.; Locher, H. H.; Seiler, P.; Ertel, E. A.; Hess, P.; Enderlin-Paput, M.; Enderlin-Paput, S.; Gauvin, J.-C.; Mirre, A.; Hubschwerlen, C.; Ritz, D.; Rueedi, G. Synthesis and Characterization of Tetrahydropyran-Based Bacterial Topoisomerase Inhibitors with Antibacterial Activity against Gram-Negative Bacteria. *J. Med. Chem.* **2017**, *60* (9), 3776−3794.

(11) Schrodinger, LLC. *Glide*, Version 86013; Schrodinger, LLC: New York, NY, 2020.

(12) Kim, S. S.; Aprahamian, M. L.; Lindert, S. Improving inverse docking target identification with Z-score selection. *Chem. Biol. Drug Des.* **2019**, *93* (6), 1105−1116.

(13) Casey, F. P.; Pihan, E.; Shields, D. C. Discovery of small molecule inhibitors of protein-protein interactions using combined ligand and target score normalization. *J. Chem. Inf. Model.* **2009**, *49* (12), 2708−2717.

(14) Liu, S.; Fu, R.; Zhou, L.-H.; Chen, S.-P. Application of consensus scoring and principal component analysis for virtual screening against beta-secretase (BACE-1). *PLoS One* **2012**, *7* (6), No. e38086.

(15) Richter, M. F.; Drown, B. S.; Riley, A. P.; Garcia, A.; Shirai, T.; Svec, R. L.; Hergenrother, P. J. Predictive compound accumulation

rules yield a broad-spectrum antibiotic. *Nature* **2017**, *545* (7654), 299−304.
(16) Constantin, T.; Zanini, M.; Regni, A.; Sheikh, N. S.; Juliá, F.; Leonori, D. Aminoalkyl radicals as halogen-atom transfer agents for activation of alkyl and aryl halides. *Science* **2020**, *367* (6481), 1021−1026.
(17) Lu, Y.; Vibhute, S.; Li, L.; Okumu, A.; Ratigan, S. C.; Nolan, S.; Papa, J. L.; Mann, C. A.; English, A.; Chen, A.; Seffernick, J. T.; Koci, B.; Duncan, L. R.; Roth, B.; Cummings, J. E.; Slayden, R. A.; Lindert, S.; McElroy, C. A.; Wozniak, D. J.; Yalowich, J.; Mitton-Fry, M. J. Optimization of TopoIV Potency, ADMET Properties, and hERG Inhibition of 5-Amino-1,3-dioxane-Linked Novel Bacterial Topoisomerase Inhibitors: Identification of a Lead with In Vivo Efficacy against MRSA. *J. Med. Chem.* **2021**, *64* (20), 15214−15249.
(18) Clinical and Laboratory Standards Institute (CLSI). *Methods for Dilution Antimicrobial Susceptibility Tests for Bacteria That Grow Aerobically; Approved Standard*, 11the ed.; CLSI standard M07; CLSI: Wayne, PA, 2018.
(19) Germe, T.; Vörös, J.; Jeannot, F.; Taillier, T.; Stavenger, R. A.; Bacqué, E.; Maxwell, A.; Bax, B. D. A New Class of Antibacterials, the Imidazopyrazinones, Reveal Structural Transitions Involved in DNA Gyrase Poisoning and Mechanisms of Resistance. *Nucleic Acids Res.* **2018**, *46* (8), 4114−4128.
(20) Cumming, J. G.; Kreis, L.; Kühne, H.; Wermuth, R.; Vercruysse, M.; Kramer, C.; Rudolph, M. G.; Xu, Z. Discovery of a series of Indane-containing NBTIs with activity against multidrug-resistant gram-negative pathogens. *ACS Med. Chem. Lett.* **2023**, *14* (7), 993−998.
(21) Fàbrega, A.; Vila, J. *Salmonella enterica* Serovar Typhimurium Skills to Succeed in the Host: Virulence and Regulation. *Clin. Microbiol. Rev.* **2013**, *26* (2), 308−341.
(22) Akshay, S. D.; Deekshit, V. K.; Raj, J. M.; Maiti, B. Outer membrane proteins and efflux pumps mediated multi-drug resistance in *Salmonella*: Rising threat to antimicrobial therapy. *ACS Infect. Dis.* **2023**, *9* (11), 2072−2092.
(23) Porwollik, S.; Santiviago, C. A.; Cheng, P.; Long, F.; Desai, P.; Fredlund, J.; Srikumar, S.; Silva, C. A.; Chu, W.; Chen, X.; Canals, R.; Reynolds, M. M.; Bogomolnaya, L.; Shields, C.; Cui, P.; Guo, J.; Zheng, Y.; Endicott-Yazdani, T.; Yang, H.-J.; Maple, A.; Ragoza, Y.; Blondel, C. J.; Valenzuela, C.; Andrews-Polymenis, H.; McClelland, M. Defined Single-Gene and Double-Gene Deletion Mutant Collections in *Salmonella enterica* sv Typhimurium. *PLoS One* **2014**, *9* (7), No. e99820.
(24) Maloy, S. R.; Stewart, V. J.; Taylor, R. K. *Genetic analysis of pathogenic bacteria: a laboratory manual*; Cold Spring Harbor Laboratory Press: Plainville, NY, 1996.
(25) Li, L.; Okumu, A.; Nolan, S.; English, A.; Vibhute, S.; Lu, Y.; Hervert-Thomas, K.; Seffernick, J. T.; Azap, L.; Cole, S. L.; Shinabarger, D.; Koeth, L. M.; Lindert, S.; Yalowich, J. C.; Wozniak, D. J.; Mitton-Fry, M. J. 1,3-dioxane-linked bacterial topoisomerase inhibitors with enhanced antibacterial activity and reduced hERG inhibition. *ACS Infect. Dis.* **2019**, *5* (7), 1115−1128.

https://doi.org/10.1021/acsmedchemlett.4c00162
ACS Med. Chem. Lett. 2024, 15, 1287−1297